Color constancy through inverse-intensity chromaticity space

Robby T. Tan

Department of Computer Science, The University of Tokyo, 4-6-1 Komaba, Meguro-ku, Tokyo, 153-8505, Japan

Ko Nishino

Department of Computer Science, Columbia University, 1214 Amsterdam Avenue, MC 0401 New York, New York 10027

Katsushi Ikeuchi

Department of Computer Science, The University of Tokyo, 4-6-1 Komaba, Meguro-ku, Tokyo, 153-8505, Japan

Received April 21, 2003; revised manuscript received September 15, 2003; accepted November 4, 2003

Existing color constancy methods cannot handle both uniformly colored surfaces and highly textured surfaces in a single integrated framework. Statistics-based methods require many surface colors and become error prone when there are only a few surface colors. In contrast, dichromatic-based methods can successfully handle uniformly colored surfaces but cannot be applied to highly textured surfaces, since they require precise color segmentation. We present a single integrated method to estimate illumination chromaticity from single-colored and multicolored surfaces. Unlike existing dichromatic-based methods, the proposed method requires only rough highlight regions without segmenting the colors inside them. We show that, by analyzing highlights, a direct correlation between illumination chromaticity and image chromaticity can be obtained. This correlation is clearly described in "inverse-intensity chromaticity space," a novel two-dimensional space that we introduce. In addition, when Hough transform and histogram analysis is utilized in this space, illumination chromaticity can be estimated robustly, even for a highly textured surface.

OCIS codes: 150.0150, 150.2950.

1. INTRODUCTION

The spectral energy distribution of light reflected from an object is the product of the illumination spectral energy distribution and the surface spectral reflectance. As a result, the color of an object observed in an image is not the actual color of the object's surface. Recovering the actual surface color requires the capability to discount the color of illumination. A computational approach to recover the actual color of objects is referred to as a color constancy algorithm.

Human perception inherently has the capability of color constancy. This capability plays important roles in object recognition processes. Unfortunately, up to now, the mechanism of human perception color constancy has not been well understood. For machine vision, color constancy is essential for various applications, such as color-based object recognition, color reproduction, image retrieval, reflection components separation, etc. This has motivated researchers in the field of machine vision to develop various color constancy methods.

Previous work. Finlayson and Schaefer[1] categorized color constancy methods into two classes: statistics-based and physics-based methods. Statistics-based methods utilize the relationship between color distributions and statistical knowledge of common lights and surfaces.[2–8] One drawback of these methods is that they require many colors to be observed on the target surfaces. On the other hand, physics-based methods,[9–13] whose algorithms are based on understanding the physical process of reflected light, can successfully deal with fewer surface colors, even to the extreme of a single surface color.[1,14] In addition, based on the surface type of the input image, physics-based methods can be divided into two groups: diffuse-based and dichromatic-based methods. Diffuse-based methods assume that input images have only diffuse reflection, while dichromatic-based methods assume that both diffuse and specular reflections occur in the images. Geusebroek *et al.*[15,16] proposed a physical basis of color constancy by considering the spectral and spatial derivatives of the Lambertian image formation model. Andersen and Granum[17] provided an analysis on image chromaticity under two illumination colors for dichromatic surfaces. Since our aim is to develop an algorithm that is able to handle both single and multiple surface colors, we will concentrate our discussion in this section on existing physics-based methods, particularly dichromatic-based methods.

Methods in dichromatic-based color constancy rely on the dichromatic reflection model proposed by Shafer.[18] Klinker *et al.*[19,20] introduced a method to estimate illumination color from a uniform colored surface by extracting a T-shape color distribution in RGB space. However, in

real images, it becomes quite difficult to extract the T shape as a result of noise, thereby making the final estimate unreliable.

Lee[11] introduced a method to estimate illumination chromaticity using highlights of at least two surface colors. The estimation is accomplished by finding an intersection of two or more dichromatic lines in chromaticity space. While this simple approach based on the physics of reflected light provides a handy method for color constancy, it suffers from a few drawbacks. First, to create the dichromatic line for each surface color from highlights, one needs to segment the surface colors beneath the highlights. This color segmentation is difficult when the target object is highly textured. Second, nearly parallel dichromatic lines caused by similar surface colors can make the intersection sensitive to noise. Consequently, for real images, which usually suffer from noise, the estimation for similar surface colors becomes unstable. Third, the method does not deal with uniformly colored surfaces. Parallel to this, several methods have been proposed in the literature.[8,21,22]

Recently, three methods have been proposed that extend Lee's algorithm[12]: Lehmann and Palm[23] developed a more robust technique to identify the dichromatic lines in chromaticity space. The success of this technique depends on an assumption that, in each highlight region, the surface color is uniform. As a consequence, the technique fails when dealing with complex textured surfaces, which usually have more than one surface color in their highlight regions. Finlayson and Schaefer[24] proposed imposing a constraint on the colors of illumination. This constraint is based on the statistics of natural illumination colors, and it improves the stability in obtaining the intersection, i.e., it addresses the second drawback of Lee's method. Furthermore, Finlayson and Schaefer[1] proposed the use of the Planckian locus as a constraint to accomplish illumination estimation from uniformly colored surfaces. This Planckian constraint on the illumination chromaticity makes the estimation more robust, especially for natural scene images. However, the method still has a few drawbacks. First, the position and the shape of the Planckian locus in chromaticity space make the estimation error prone to certain surface colors, such as blue or yellow. Second, as they include diffuse regions in obtaining dichromatic lines, the result could become inaccurate. While the fact that the method of Finlayson and Schaefer[1] does not require reflection separation is one of the advantages, the diffuse cluster usually has a different direction from that of the specular cluster because of noise; as a result, the dichromatic line can be shifted from the correct one. Third, like other previous methods, color segmentation is required for multicolored surfaces.

Contributions. In this paper, our goal is to accomplish illumination chromaticity estimation for single-colored and multicolored surfaces based on a dichromatic reflection model. Briefly, the method is as follows. Given a single colored image, we estimate rough highlight regions by thresholding on brightness and saturation values. We transform the pixels of the estimated highlight regions into inverse-intensity chromaticity space, a novel space that we introduce. In this space, the correlation between image chromaticity and illumination chromaticity becomes linear. As a result, based on this linear correlation, we are able to estimate illumination chromaticity for both single-colored and multicolored surfaces, without segmenting the color underneath the highlights. In addition, we use Hough transform and histogram analysis for accurate and robust estimation.

In comparison with Lee's method,[12] the method has two advantages: First, it does not require multicolored surfaces, and second, it does not suffer from the problem of similar surface colors. It also advances the method of Lehmann and Palm,[23] since it does not assume that the surface color underneath a highlight region is uniform, as well as being feasible even for uniformly colored surfaces. Moreover, unlike the dichromatic method of Finlayson and Schaefer,[1] the method does not require known camera sensitivity and a strong constraint on illumination such as a blackbody radiator. Basically, this paper provides two main contributions. First, it presents a single integrated method that can be applied for both uniformly colored surfaces and highly textured surfaces. Second, it introduces an inverse-intensity chromaticity space that clearly describes the linear correlation between image chromaticity and illumination chromaticity.

Note that, while having the ability to work on a rough estimate of highlight regions is one of the advantages of our method, the problem of identifying highlight regions is still an open and challenging problem. Moreover, although the method does not require any other intrinsic camera characteristics, such as sensor sensitivity as well as the assumption of a narrowband sensor, it assumes that the output of the camera is linear to the flux of incoming light.

The remaining discussion of the paper is organized as follows. In Section 2, the reflection model of inhomogeneous materials and image color formation is discussed. In Section 3, we explain the theoretical derivation of the correlation between image chromaticity and illumination chromaticity. In Section 4, we apply the theoretical derivation in a practical computational method to estimate illumination chromaticity. In Section 5, the distribution in inverse-intensity chromaticity space is discussed in detail in order to understand the main factors that determine the robustness of the estimation. We provide a brief description of the implementation, the experimental results, and the evaluations for real images in Section 6. Finally, in Section 7, we conclude our paper.

2. REFLECTION MODEL

Optically, most objects can be divided into two categories: homogeneous and inhomogeneous objects. Homogeneous objects, which have a uniform refractive index throughout their surface and body, produce only specular reflection.[25] On the contrary, inhomogeneous objects, which have varying refractive indices in their surface and body, exhibit diffuse reflection. In addition, because of the refractive-index difference between the object's surfaces and the air, inhomogeneous objects also reflect specular reflection.[18] The amount of the reflected light is governed by Fresnel's law, while the direction of the specular reflection is relative to the local surface normal. Thus reflection of

opaque inhomogeneous objects can be modeled as a linear combination of diffuse and specular reflections, which is known as the dichromatic reflection model.[18] The model states that the light reflected from an object is a linear combination of diffuse and specular reflections:

$$I(\lambda, \bar{\mathbf{x}}) = w_d(\bar{\mathbf{x}})S_d(\lambda, \bar{\mathbf{x}})E(\lambda, \bar{\mathbf{x}}) + w_s(\bar{\mathbf{x}})S_s(\lambda, \bar{\mathbf{x}})E(\lambda, \bar{\mathbf{x}}), \quad (1)$$

where $\bar{\mathbf{x}} = \{r, s, t\}$ is the position of a surface point in a three-dimensional world coordinate system and $w_d(\bar{\mathbf{x}})$ and $w_s(\bar{\mathbf{x}})$ are the geometrical parameters for diffuse and specular reflection, respectively, whose values depend on the geometric structure at location $\bar{\mathbf{x}}$. $S_d(\lambda, \bar{\mathbf{x}})$ is the diffuse spectral reflectance function, $S_s(\lambda, \bar{\mathbf{x}})$ is the specular spectral reflectance function, and $E(\lambda, \bar{\mathbf{x}})$ is the spectral energy distribution function of the illumination.

For most dielectric inhomogeneous objects, the spectral reflectance distribution of the specular reflection component is similar to the spectral energy distribution of the incident light.[24] Researchers usually assume that both are the same.[1,9,12,22] Lee *et al.*[26] named this well-known assumption the neutral interface reflection assumption. All dichromatic-based methods, including our method, use this assumption as one of the basic assumptions. As a result, we can set $S_s(\lambda, \bar{\mathbf{x}})$ as a constant, and Eq. (1) becomes

$$I(\lambda, \bar{\mathbf{x}}) = w_d(\bar{\mathbf{x}})S_d(\lambda, \bar{\mathbf{x}})E(\lambda, \bar{\mathbf{x}}) + \tilde{w}_s(\bar{\mathbf{x}})E(\lambda, \bar{\mathbf{x}}), \quad (2)$$

where $\tilde{w}_s(\bar{\mathbf{x}}) = w_s(\bar{\mathbf{x}})k_s(\bar{\mathbf{x}})$, with $k_s(\bar{\mathbf{x}})$ being a constant scalar with respect to the wavelength.

Image formation. An image taken by a digital color camera can be described as

$$I_c(\mathbf{x}) = w_d(\mathbf{x})\int_\Omega S_d(\lambda, \mathbf{x})E(\lambda)q_c(\lambda)\mathrm{d}\lambda + \tilde{w}_s(\mathbf{x})\int_\Omega E(\lambda)q_c(\lambda)\mathrm{d}\lambda, \quad (3)$$

where I_c is the sensor response (RGB pixel values), which in this paper we call image intensity, $\mathbf{x} = \{x, y\}$ stands for the two-dimensional image coordinates, and q_c is the three-element-vector of sensor sensitivity with index c representing the type of sensor (r, g, and b). The integration is done over the visible spectrum (Ω). Note that we ignore camera noise and gain. In addition, we assume a uniform color of illumination over the input image, so that the illumination spectral distribution $E(\lambda)$ becomes independent of the image coordinate ($\mathbf{x}$). For the sake of simplicity, Eq. (3) is written as

$$I_c(\mathbf{x}) = w_d(\mathbf{x})B_c(\mathbf{x}) + \tilde{w}_s(\mathbf{x})G_c, \quad (4)$$

where $B_c(\mathbf{x}) = \int_\Omega S_d(\lambda, \mathbf{x})E(\lambda)q_c(\lambda)\mathrm{d}\lambda$ and $G_c = \int_\Omega E(\lambda)q_c(\lambda)\mathrm{d}\lambda$. The first part of the right-hand side of the equation represents the diffuse reflection component, while the second part represents the specular reflection component.

3. INVERSE-INTENSITY CHROMATICITY SPACE

In this paper, chromaticity, also commonly called normalized rgb, is defined as

$$\sigma_c(\mathbf{x}) = \frac{I_c(\mathbf{x})}{\sum I_i(\mathbf{x})}, \quad (5)$$

where $\Sigma I_i(\mathbf{x}) = I_r(\mathbf{x}) + I_g(\mathbf{x}) + I_b(\mathbf{x})$.

If we consider the chromaticity definition in the last equation and the image intensity definition in Eq. (4), for the diffuse-only reflection component ($\tilde{w}_s = 0$), the chromaticity becomes independent of the diffuse geometrical parameter w_d, since it is factored out by using Eq. (5). We call this diffuse chromaticity (Λ_c), with the definition

$$\Lambda_c(\mathbf{x}) = \frac{B_c(\mathbf{x})}{\sum B_i(\mathbf{x})}. \quad (6)$$

On the other hand, for the specular-only reflection component ($w_d = 0$), the chromaticity is independent of the specular geometrical parameter ($\tilde{w}_s$), which we call specular chromaticity (Γ_c):

$$\Gamma_c = \frac{G_c}{\sum G_i}. \quad (7)$$

Consequently, by considering Eqs. (6) and (7), we can write Eq. (4) as

$$I_c(\mathbf{x}) = m_d(\mathbf{x})\Lambda_c(\mathbf{x}) + m_s(\mathbf{x})\Gamma_c, \quad (8)$$

where

$$m_d(\mathbf{x}) = w_d(\mathbf{x})\sum B_i(\mathbf{x}), \quad (9)$$

$$m_s(\mathbf{x}) = \tilde{w}_d(\mathbf{x})\sum G_i. \quad (10)$$

We can also set $\Sigma\sigma_i(\mathbf{x}) = \Sigma\Lambda_i(\mathbf{x}) = \Sigma\Gamma_i = 1$, without loss of generality. Note that we assume that the camera output is linear to the flux of incoming light intensity, since, in our method, only by using that assumption can the above chromaticity definitions be applied to estimate illumination chromaticity.

A. Image Chromaticity and Image Intensity

By replacing each channel's image intensity in Eq. (5) with its definition in Eq. (8) and considering pixel-based operation, we can write the image chromaticity in terms of a dichromatic reflection model:

$$\sigma_c = \frac{m_d\Lambda_c + m_s\Gamma_c}{m_d\sum \Lambda_i + m_s\sum \Gamma_i}. \quad (11)$$

By deriving the last equation, we can obtain the correlation between m_s and m_d:

$$m_s = \frac{m_d(\Lambda_c - \sigma_c)}{\sigma_c - \Gamma_c}. \quad (12)$$

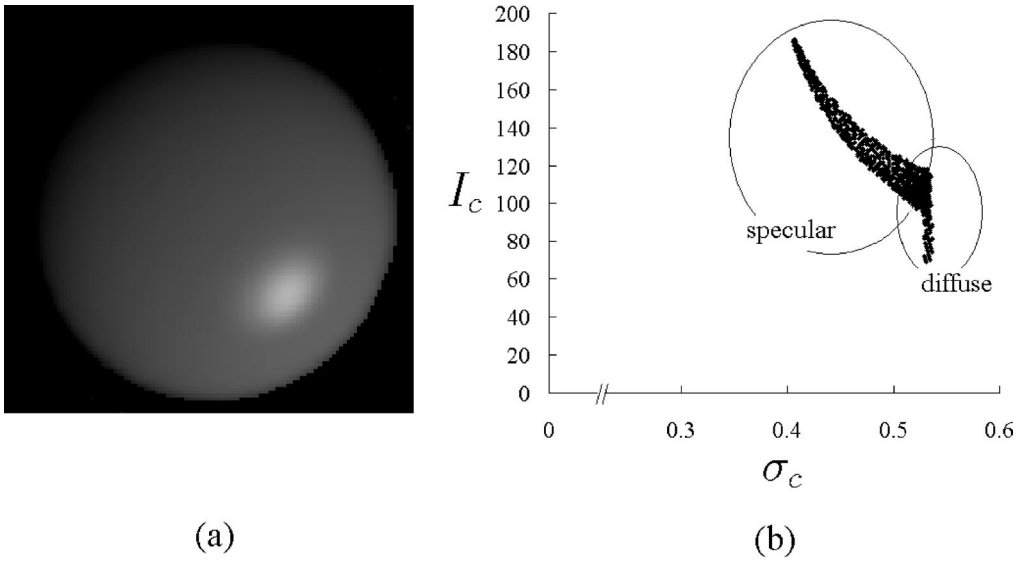

Fig. 1. (a) Synthetic image with a single surface color; (b) projection of the diffuse and specular pixels into the chromaticity-intensity space, with c representing the green channel.

Then, by plugging Eq. (12) into Eq. (8), we can describe the correlation between image intensity (I_c) and image chromaticity (σ_c) as

$$I_c = m_d(\Lambda_c - \Gamma_c)\left(\frac{\sigma_c}{\sigma_c - \Gamma_c}\right). \tag{13}$$

The last equation shows that the correlation between image intensity (I_c) and image chromaticity (σ_c) is not linear.

If a uniformly colored surface is projected into chromaticity-intensity space, according to Eq. (13), the specular pixels will form a curved cluster (nonlinear correlation), as illustrated in Fig. 1(b). On the other hand, the diffuse pixels will form a straight vertical line, since image chromaticity (σ_c), which equals diffuse chromaticity (Λ_c), is independent of image intensity (I_c).

B. Image Chromaticity and Illumination Chromaticity

By introducing p, which we define as $p = m_d(\Lambda_c - \Gamma_c)$, we can derive from Eq. (13) that

$$\frac{I_c}{\sigma_c} = \frac{p}{\sigma_c - \Gamma_c}. \tag{14}$$

Since $I_c/\sigma_c = \Sigma I_i$, then the correlation between image chromaticity and illumination chromaticity becomes

$$\sigma_c = p\frac{1}{\sum I_i} + \Gamma_c. \tag{15}$$

This equation is the core of our method. It shows that by solely calculating the value of p, we are able to determine the illumination chromaticity (Γ_c), since image chromaticity (σ_c) and total image intensity (ΣI_i) can be directly observed from the input image. The details are as follows.

If the values of p are constant and the values of ΣI_i vary throughout the image, the last equation becomes a linear equation, and the illumination chromaticity (Γ_c) can be estimated in a straightforward manner by using general line-fitting algorithms. However, in most images, the values of p are not constant, since p depends on m_d, Λ_c, and Γ_c. For the sake of simplicity, until the end of this subsection, we temporarily assume that the values of Λ_c are constant, making the values of p depend solely on m_d, as Γ_c has already been assumed to be constant.

Equation (9) states that $m_d = w_d \Sigma B_i$. According to Lambert's Law,[27] w_d is determined by the angle between lighting direction and surface normal, while ΣB_i is determined by diffuse albedo (k_d) and intensity of incident light (L). The angles between surface normals and light directions depend on the shape of the object and the light distribution. The angle will be constant if an object has a planar surface and illumination directions are all the same for all points in the surface. However, if the surface is not planar or the illumination directions are not uniform, then the angle will vary. For a surface with a uniform color, the value of the diffuse albedo (k_d) is constant. The values of L (intensity of incident light) are mostly determined by the location of illuminants, which will be constant if the locations of the illuminants are distant from the surface. For relatively nearby illuminants, the values of L may vary with respect to the surface point. With all these aspects taken into consideration, in general conditions, then, the value of m_d can be either constant or varied. Yet, in most cases, the value of m_d will be varied because most shapes of objects in the real world are not planar and the assumption on uniform illumination direction, in some conditions, cannot be held.

Consequently, Eq. (15) poses two problems: first, whether there are a number of specular pixels that have the same m_d, and second, whether these pixels that have the same m_d also have different ΣI_i. If we consider a single surface color, then the solution of the first problem depends on w_d and L. In the microscopic scale of the real world, the combination of w_d and L could be unique for

certain circumstances. Fortunately, in the scale of image intensity, for some set of surface points, the differences between combinations of w_d and L are small and can be approximated as constant. We can take this approximation for granted, as current ordinary digital cameras automatically do it for us as a part of their accuracy limitation. Moreover, in Section 5, we will explain that the distribution of specular pixels for the same surface color is localized in a certain area in inverse-intensity chromaticity space, in which certain points have small differences in p and thus can be grouped together.

The second problem can be resolved by considering Eq. (8). In this equation, two specular pixels will have the same m_d but different I_c if their values of m_s are different. Equation (10) states that $m_s = \tilde{w}_s \Sigma G_i$. In the Torrance and Sparrow reflection model,[28] which is reasonably accurate for modeling specularity, $\tilde{w}_s$ is expressed as

$$\tilde{w}_s = FG \frac{1}{\cos \theta_r} \exp\left(-\frac{\alpha^2}{2\phi^2} \right), \tag{16}$$

where F is the Fresnel reflection, G is the geometrical attenuation factor, θ_r is the angle between the surface normal and the viewing direction, α is the angle between the surface normal and the bisector of viewing direction and illumination direction, and ϕ is the surface roughness. Thus, if the two specular pixels have the same surface color lit by a distant light source and have the same m_d, which implies the same p, then the m_s of both pixels will be different if their values of θ_r and α are different.

Hence, in general conditions, specular pixels can be grouped into a number of clusters that have the same values of p and different ΣI_i. For every group of pixels that share the same value of m_d, we can consider p a constant, which makes Eq. (15) linear, with p as its constant gradient. These groups of pixels can be clearly observed in inverse-intensity chromaticity space, where its x axis represents $1/\Sigma I_i$ and its y axis represents σ_c, as illustrated in Fig. 2(a). Several straight lines in the figure correspond to several groups of different m_d values (several numbers of p: $p_1, \ldots, p_j, \ldots, p_n$). These lines intersect at a single point on the y axis, which is identical to the illumination chromaticity (Γ_c). Figure 3(a) shows the projection of all pixels of a synthetic image in Fig. 1(a) into inverse-intensity chromaticity space. The horizontal line in the figure represents the diffuse points, since the image chromaticity of diffuse pixels will be constant regardless of the change of ΣI_i, whereas the slanted cluster represents the specular points. If we focus on this cluster by removing the diffuse points, then, according to Eq. (15), we will find that a number of straight lines, which compose the cluster, head for the value of illumination chromaticity at the y axis, as shown in Fig. 3(b).

Now we relax the assumption of a uniformly colored surface to handle multicolored surfaces. Figure 2(b) illustrates the projection of two different surface colors into inverse-intensity chromaticity space. We can observe that two specular clusters with different values of diffuse chromaticity head for the same value on the chromaticity axis (Γ_c). Since we consider only points that have the same values of p and Γ_c, then even if there are many different clusters with different values of Λ_c, as is the case for multicolored surfaces, we can still safely estimate the illumination chromaticity (Γ_c). This means that, for multicolored surfaces, the estimation process is exactly the same as that in the case of a uniformly colored surface. Figure 4(b) shows the projection of highlight regions of a synthetic image with two surface colors [Fig. 4(a)] into inverse-intensity chromaticity space.

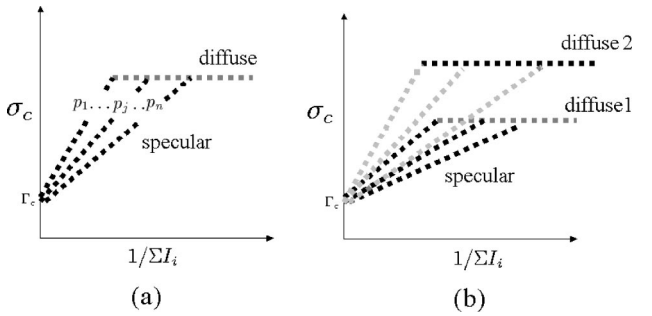

Fig. 2. (a) Sketch of specular points of a uniformly colored surface in inverse-intensity chromaticity space, (b) sketch of specular points of two different surface colors.

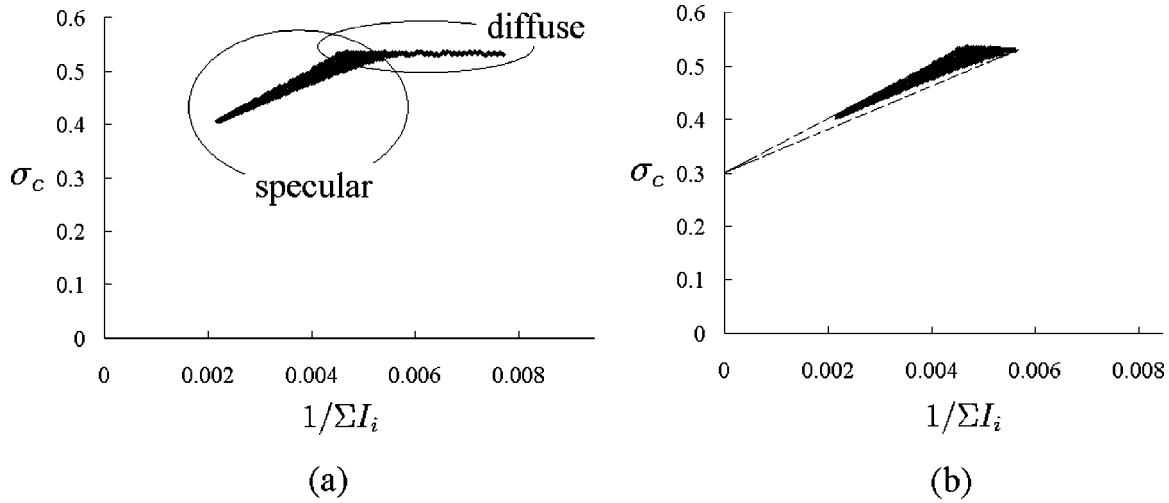

Fig. 3. (a) Diffuse and specular points of a synthetic image [Fig. 1(a)] in inverse-intensity chromaticity space, with c representing the green channel; (b) cluster of specular points that head for the illumination-chromaticity value in the y axis.

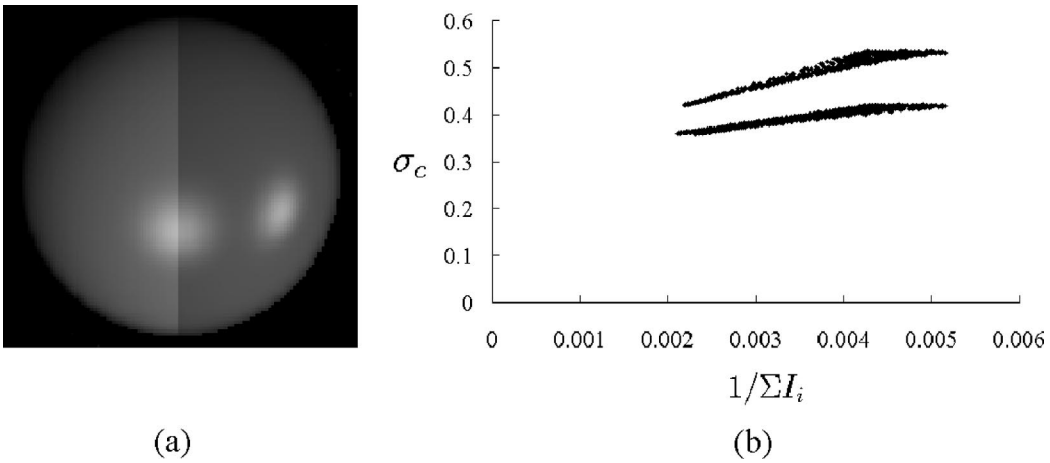

Fig. 4. (a) Synthetic image with multiple surface colors; (b) specular points in inverse-intensity chromaticity space, with c representing the green channel.

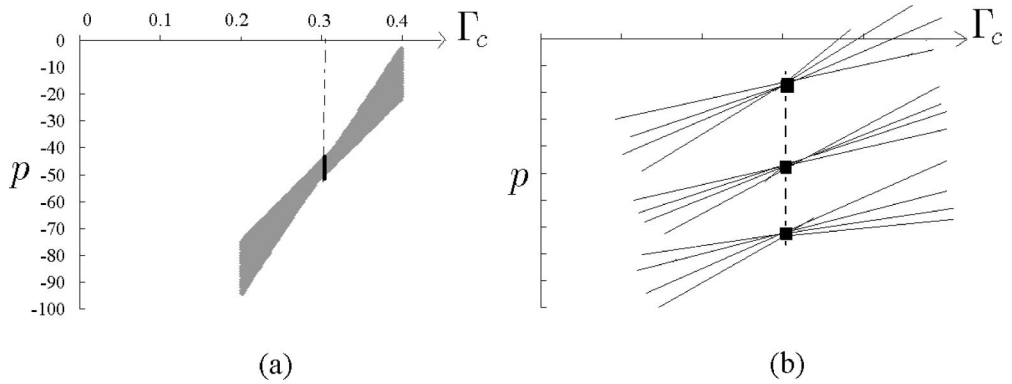

Fig. 5. (a) Projection of points in Fig. 3(b) into Hough space, (b) sketch of intersected lines in Hough space.

4. COMPUTATIONAL METHOD TO ESTIMATE ILLUMINATION CHROMATICITY

To estimate the illumination chromaticity (Γ_c) from inverse-intensity chromaticity space, we use the Hough transform. Figure 5(a) shows the transformation from inverse-intensity chromaticity space into Hough space, where its x axis represents Γ_c and its y axis represents p. Since Γ_c is a normalized value, the range of its value is from 0 to 1 ($0 < \Gamma_c < 1$).

Using the Hough transform alone does not yet give any solution, because the values of p are not constant throughout the image, which causes the intersection point of lines not to be located at a single location. Fortunately, even if the values of p vary, the values of Γ_c are constant. Thus, in principle, all intersections will be concentrated at a single value of Γ_c, with a small range of p values. These intersections are indicated by a thick solid line in Fig. 5(a).

If we focus on the intersections in the Hough space as illustrated in Fig. 5(b), we should find a larger number of intersections at a certain value of Γ_c compared with that at other values of Γ_c. The reason is that, in inverse-intensity chromaticity space, within the range of Γ_c ($0 < \Gamma_c < 1$), the number of groups of points that form a straight line heading for a certain value of Γ_c are more dominant than the number of groups of points that form a straight line heading for other values of Γ_c.

In practice, we count the intersections in Hough space based on the number of points that occupy the same location. The details are as follows. A line in Hough space is formed by a number of points. If this line is not intersected by other lines, then each point will occupy a certain location uniquely (one point for each location). However, if two lines intersect, a location where the intersection takes place will be shared by two points. The number of points will increase if other lines also intersect with those two lines at the same location. Thus, to count the intersections, we first discard all points that occupy a location uniquely, as it means that there are no intersections, and then count the number of points for each value of Γ_c.

As a consequence, by projecting the total number of intersections of each Γ_c into a two-dimensional space (illumination-chromaticity count space), with the y axis representing the count of intersections and the x axis representing Γ_c, we can robustly estimate the actual value of Γ_c. Figure 6 shows the distribution of the count numbers of intersections in the space, where the distribution forms a Gaussian-like distribution. The peak of the distribution lies at the actual value of Γ_c.

5. DISCUSSION

In this section, we analyze the distributions of points of highlight regions in inverse-intensity chromaticity space.

This analysis is important, since by understanding the distribution, we can know the main factors that determine the accuracy and the robustness of the illumination-chromaticity estimation using the space. Note that, while in this discussion, for the sake of simplicity we assume a single surface color, the analysis results can be applied to multicolored surfaces as well.

First, we analyze the distribution when the values of m_d are constant throughout the image. For a uniformly colored surface, this constant m_d makes p identical for all specular points. As a result, the distribution of the specular pixels forms a single straight line in inverse-intensity chromaticity space, as shown in Fig. 7. $\overline{AB}$, in the figure, represents the specular line whose gradient is determined by the value of p and whose length is represented by h, i.e., the distance between the brightest specular point and the corresponding diffuse point that has the same p value. Mathematically, the value of h is determined by

$$h = \left| \frac{m_s^A}{m_d^A(m_d^A + m_s^A)} [1 + (m_d^A)^2(\Lambda_c - \Gamma_c)^2]^{1/2} \right|, \tag{17}$$

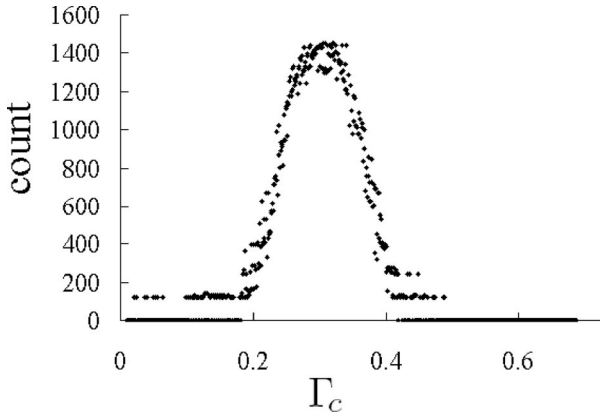

Fig. 6. Intersection-counting distribution of green channel. Estimated illumination chromaticity: $\Gamma_r = 0.535$, $\Gamma_b = 0.303$, $\Gamma_b = 0.162$; ground-truth values: $\Gamma_r = 0.536$, $\Gamma_b = 0.304$, $\Gamma_b = 0.160$.

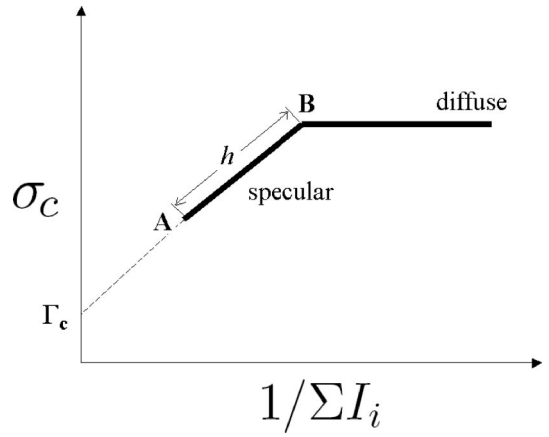

Fig. 7. Distribution of specular and diffuse pixels in inverse-intensity chromaticity space when m_d is constant.

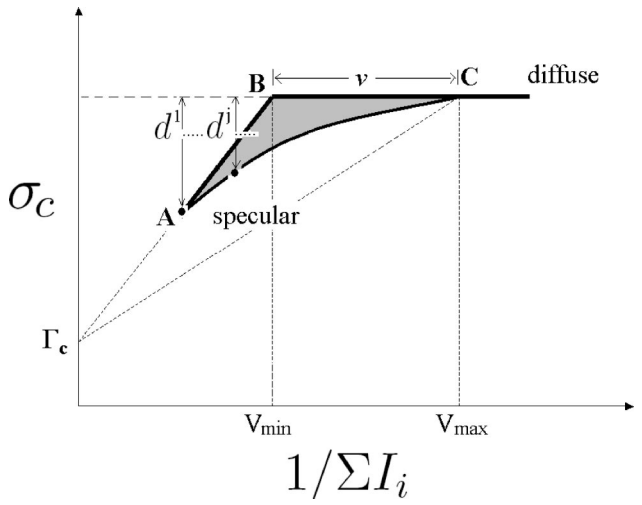

Fig. 8. Distribution of specular and diffuse pixels in inverse-intensity chromaticity space when m_d varies.

where m_s^A and m_d^A are the m_s and m_d values of the brightest specular pixel at A. The value of m_d^A is identical to the value of m_d^B.

Equation (17) implies that surface roughness, one of the components of m_s, significantly determines the value of h. Two objects that have the same shape and surface color, located at the same position, and lit by the same illumination, when viewed from the same location (the same value of m_d^B) will have different values of h if the surface roughnesses of the objects are different. The smaller surface roughness (larger value of m_s^A) will produce longer h. On the other hand, the larger surface roughness (smaller value of m_s^A) will produce shorter h. For our estimation method, the longer h is better, yet fortunately, even if h is short, as long as the highlight regions can be obtained, the illumination-chromaticity estimation can be done accurately.

Second, we analyze the distribution when the values of m_d vary throughout the image. If m_d varies, for uniformly colored surfaces, p will also vary, which consequently makes specular points in inverse-intensity chromaticity space form a number of straight lines heading for a unique value in the y axis. If the change of m_d is assumed to be continuous (smooth surface), the straight lines will grow into a cluster, as illustrated in Fig. 8. $\overline{AB}$, in the figure, represents the specular straight line from the brightest specular point to the corresponding diffuse point that has the same value of p. The length of $\overline{AB}$ is represented by h, which value is also determined by Eq. (17). Point C represents the diffuse point that has the dimmest specular pixel (but its m_s is larger than zero). The length of $\overline{BC}$ is represented by v, which equals $V_{max} - V_{min}$, where V_{max} and V_{min} are the values of inverse intensity of diffuse pixels that have identical p to the dimmest specular pixel and to the brightest specular pixel, respectively. Note that it is not necessary that the value of V_{min} be the lowest inverse-intensity value of diffuse pixels, since some diffuse pixels, in certain conditions, could have inverse-intensity values smaller than V_{min}.

The value of v, which is determined by V_{max} and V_{min}, depends not only on m_d but also on several factors that

determine the value of m_s, such as surface roughness. By considering the Torrance and Sparrow reflection model in Eq. (16), if the surface has small surface roughness, then the number of specular pixels (pixels whose m_s does not equal zero) is relatively small, which could make the diversity of m_d in highlight regions also small. On the contrary, if the same surface has large surface roughness, then the number of specular pixels is relatively large, making the diversity of m_d in highlight regions possibly large. As a result, since surface roughness affects the diversity of m_d in highlight regions, it also affects the value of v. In general cases, smaller surface roughness will cause the value of v to be smaller, while larger surface roughness will cause the value of v to be larger.

Besides the values of h and v, we also need to know the shape of the boundaries of the distribution. As explained above, the shape of $\overline{AB}$ is a straight line whose gradient equals the p of the brightest specular pixel, while the shape of $\overline{BC}$ is a straight horizontal line, since for all diffuse pixels, their image chromaticity values are identical regardless of the change of image intensity. Unlike both lines, the shape of $\overline{AC}$ in general cases is not a straight line. To know the shape of the line, we need to define the vertical distances between points at $\overline{AC}$ and the diffuse horizontal line, which is represented by d, as shown in Fig. 8. The values of d are determined by

$$d^j = \left| \frac{m_s^j}{m_d^j + m_s^j} (\Lambda_c - \Gamma_c) \right|, \tag{18}$$

where superscript j is the index of specular points located at $\overline{AC}$ and m_d^j is the diffuse pixel that has p identical to that of the corresponding specular point located at $\overline{AC}$ with index j. From Eq. (18), we can conclude that the shape of $\overline{AC}$ is a curved line, since according to the Torrance and Sparrow reflection model, m_s is a Gaussian function [Eq. (16)].

Once the factors are known that determine the distribution of specular points when m_d varies, then if the surface roughness is small, v will be small, h will be long, and $\overline{AC}$ will be more parallel to $\overline{AB}$. In this condition, the estimation using our computational method can be done accurately and robustly. On the contrary, if the surface roughness is large, then v will be large, h will be short, and $\overline{AC}$ will be more parallel to $\overline{BC}$, making the estimation in practice less robust compared with that for relatively smaller surface roughness.

6. EXPERIMENTAL RESULTS

We will briefly describe the implementation of the proposed method and then present several experimental results on real images as well as an evaluation of our method.

Implementation. Implementation of the proposed method is quite simple. Given an image that has highlights, we first find the highlight regions by using thresholding on image intensity and saturation values. Following the method of Lehmann and Palm,[23] we define the thresholding as follows:

$$\tilde{I} = \frac{I_r + I_g + I_b}{3} > T_a \tilde{I}^{\max},$$

$$\tilde{S} = 1 - \frac{\min(I_r, I_g, I_b)}{\tilde{I}} < T_b \tilde{S}^{\max}, \tag{19}$$

where $\tilde{I}^{\max}$ and $\tilde{S}^{\max}$ are the largest $\tilde{I}$ and $\tilde{S}$ in the whole input image, respectively. T_a and T_b are the thresholds of image intensity and saturation, respectively. In our implementation, we set T_a and T_b from 0.4 to 0.6.

This thresholding technique cannot always produce precise highlight regions. Fortunately, in practice, our estimation method does not need precise highlight regions; even if relatively small regions of diffuse pixels are included, the algorithm could work robustly. Of course, more preciseness is better. Then, for each color channel, we project the highlight pixels into inverse-intensity chromaticity space. From this space, we use the conventional Hough transform to project the clusters into Hough space. During the projection, we count all possible intersections at each value of chromaticity. We plot these intersection-counting numbers into the illumination-chromaticity count space. Ideally, from this space, we can choose the tip as the estimated illumination chromaticity. However, as noise always exists in real images, the result can be improved by computing the median of a certain percentage from the highest counts. In our implementation, we use 30% from the highest counted number.

Note that, first, in our current implementation we estimate three color channels of illumination chromaticity independently. In fact, since $\Sigma\Gamma_i = 1$, we can solely estimate two color channels instead of three color channels. Second, the problem of determining highlight regions is still an open and challenging problem, and our method could fail for specific domains that do not follow our thresholding described in Eqs. (19).

Experimental conditions. We have conducted several experiments on real images, which were taken with a SONY DXC-9000, a progressive 3 CCD digital camera, by setting its gamma correction off. To ensure that the output of the camera is linear to the flux of incident light, we used a spectrometer (Photo Research PR-650). We examined the algorithm by using four types of input, i.e., uniform colored surfaces, multicolored surfaces, highly textured surfaces, and a scene with multiple objects. We used convex objects to avoid interreflection and excluded saturated pixels from the computation. For evaluation, we compared the results with the average values of image chromaticity of a white reference image (Photo Research Reflectance Standard model SRS-3), captured by the same camera. The standard deviations of these average values under various illuminant positions and colors were approximately 0.01–0.03.

Result on a uniformly colored surface. Figure 9(a) shows a real image of a head model that has a uniformly colored surface and relatively low specularity, illuminated by a Solux Halogen with temperature 4700 K. Under the illumination, the image chromaticity of the white reference taken by our camera has chromaticity values $\Gamma_r = 0.371$, $\Gamma_g = 0.318$, $\Gamma_b = 0.310$.

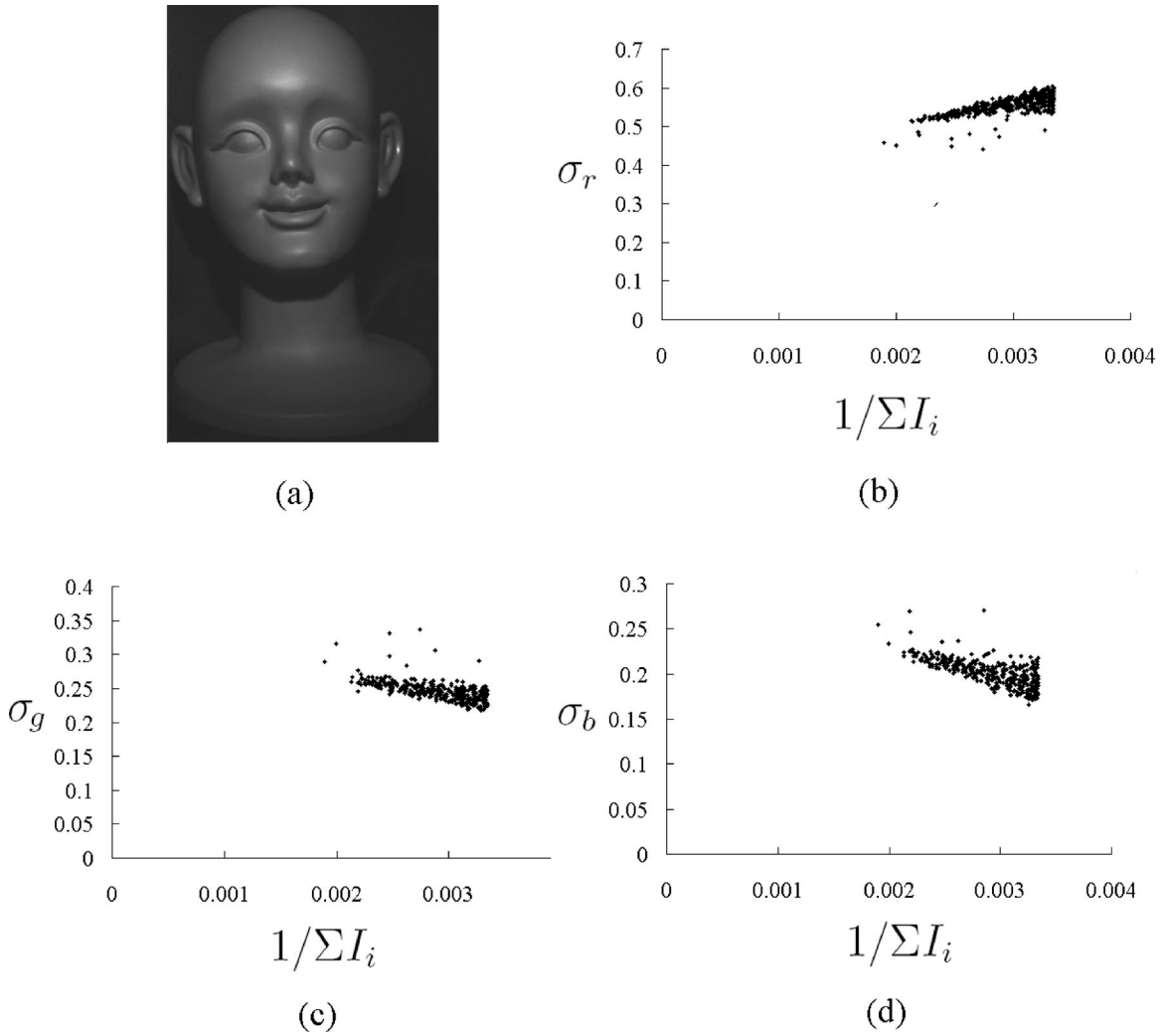

Fig. 9. (a) Real input image with a single surface color, (b) projection of the red channel of the specular pixels into inverse-intensity chromaticity space, (c) projection of the green channel of the specular pixels into inverse-intensity chromaticity space, (d) projection of the blue channel of the specular pixels into inverse-intensity chromaticity space.

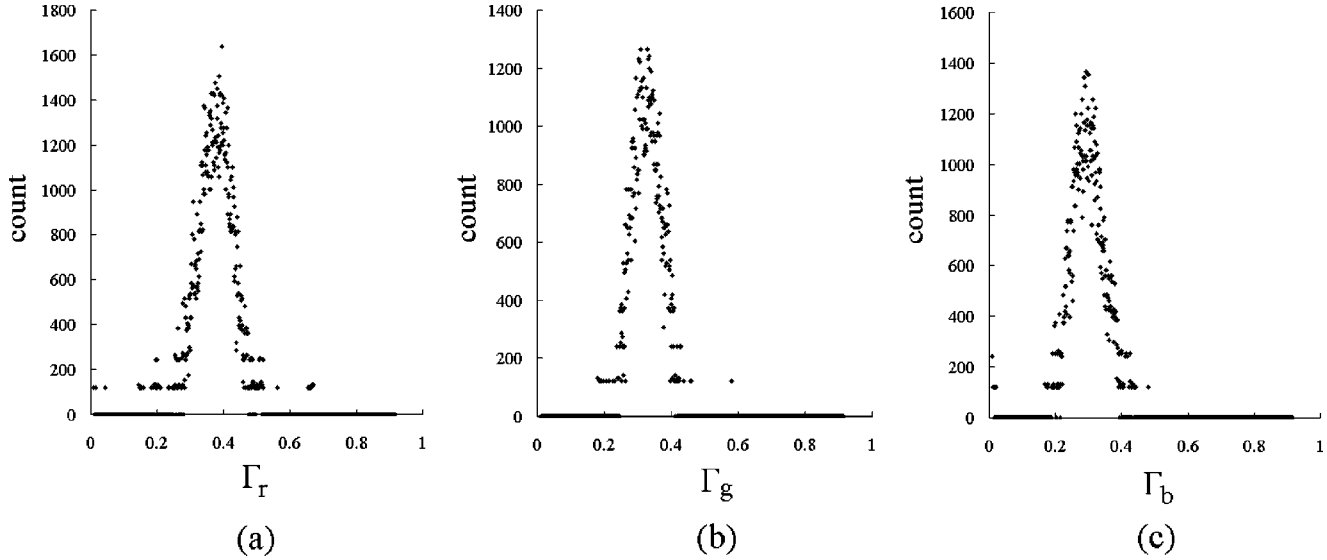

Fig. 10. (a) Intersection-counting distribution for the red channel of illumination chromaticity for the image in Fig. 9, (b) intersection-counting distribution for the green channel, (c) intersection-counting distribution for the blue channel.

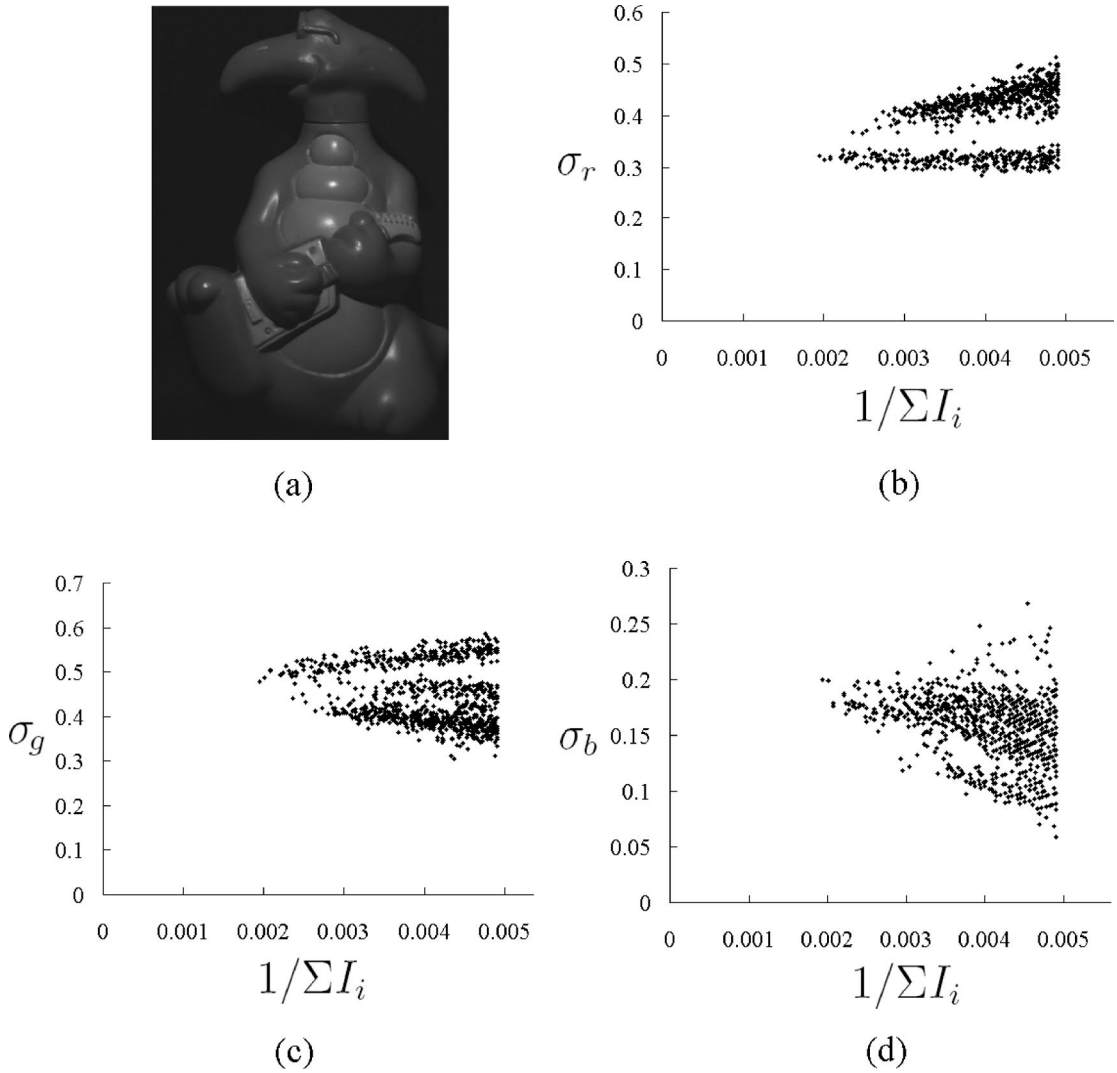

Fig. 11. (a) Real input image with multiple surface colors, (b) projection of the red channel of the specular pixels into inverse-intensity chromaticity space, (c) projection of the green channel of the specular pixels into inverse-intensity chromaticity space, (d) projection of the blue channel of the specular pixels into inverse-intensity chromaticity space.

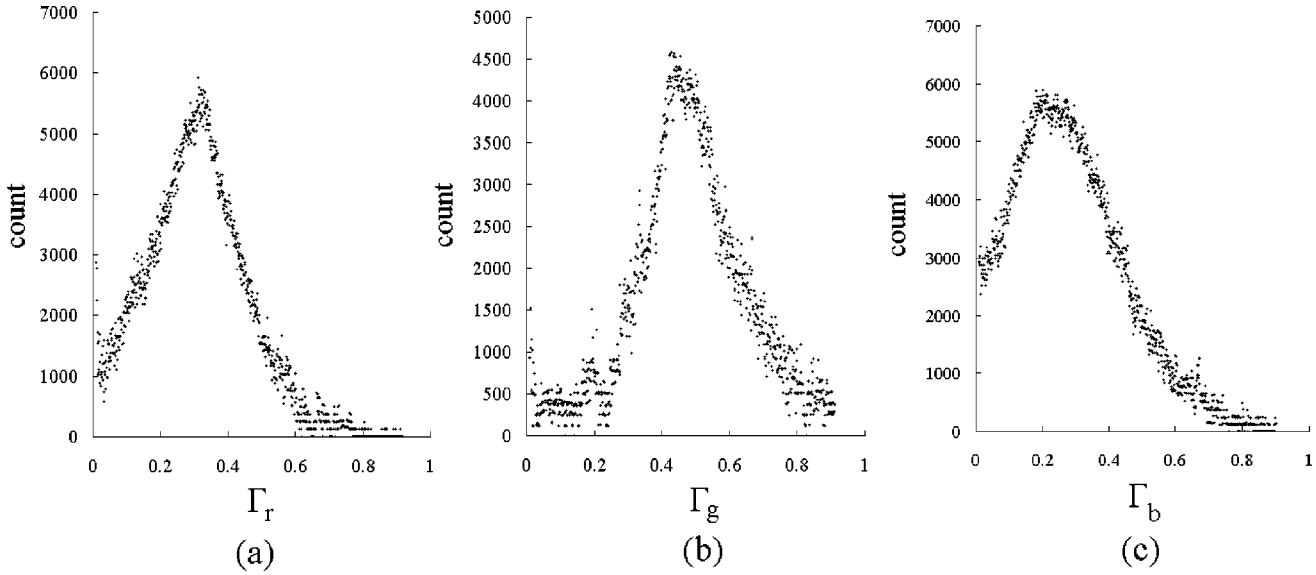

Fig. 12. (a) Intersection-counting distribution for the red channel of illumination chromaticity for the image in Fig. 11, (b) intersection-counting distribution for the green channel, (c) intersection-counting distribution for the blue channel.

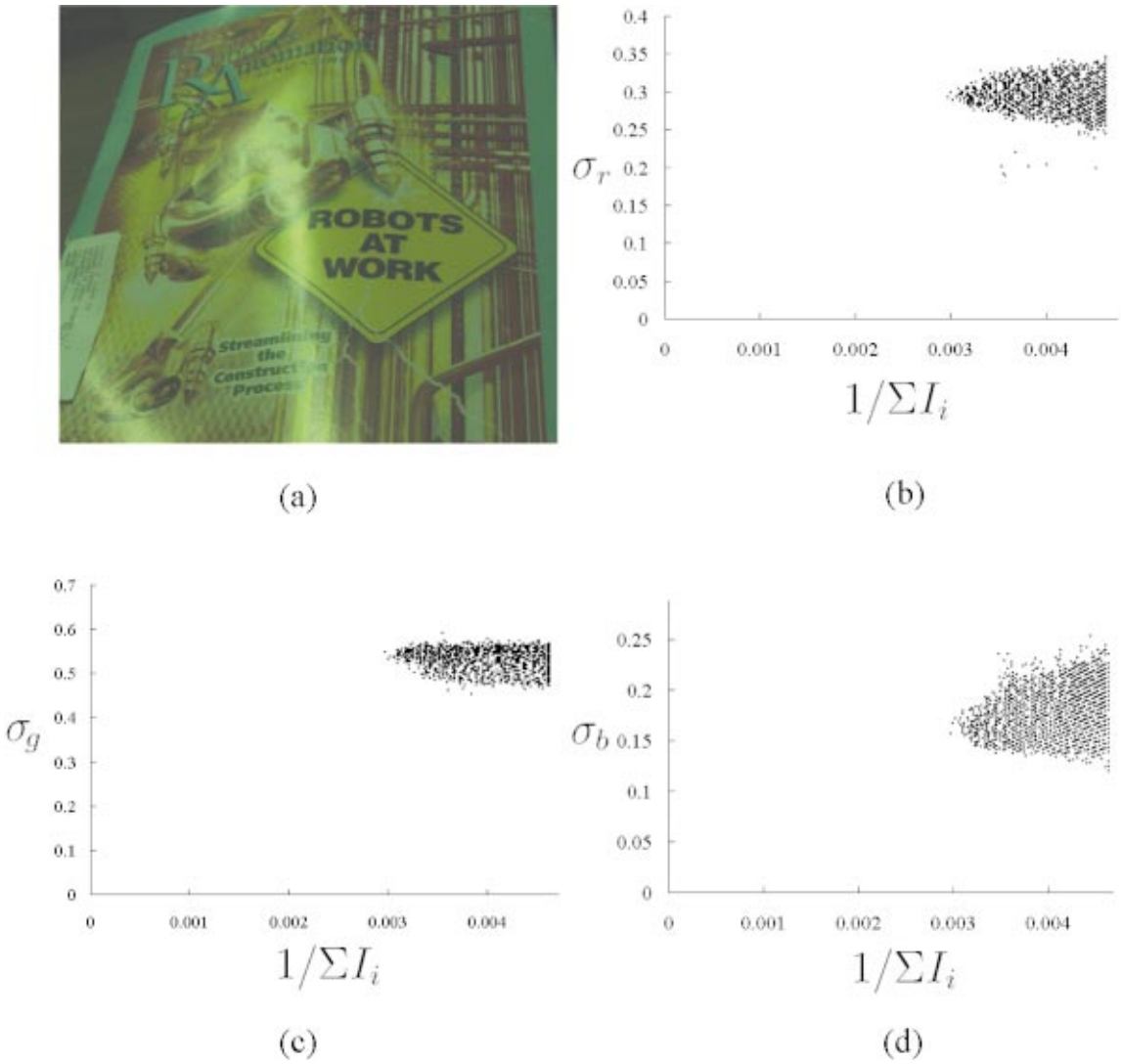

Fig. 13. (a) Real input image of complex textured surface, (b) projection of the red channel of the specular pixels into inverse-intensity chromaticity space, (c) projection of the green channel of the specular pixels into inverse-intensity chromaticity space, (d) projection of the green channel of the specular pixels into inverse-intensity chromaticity space.

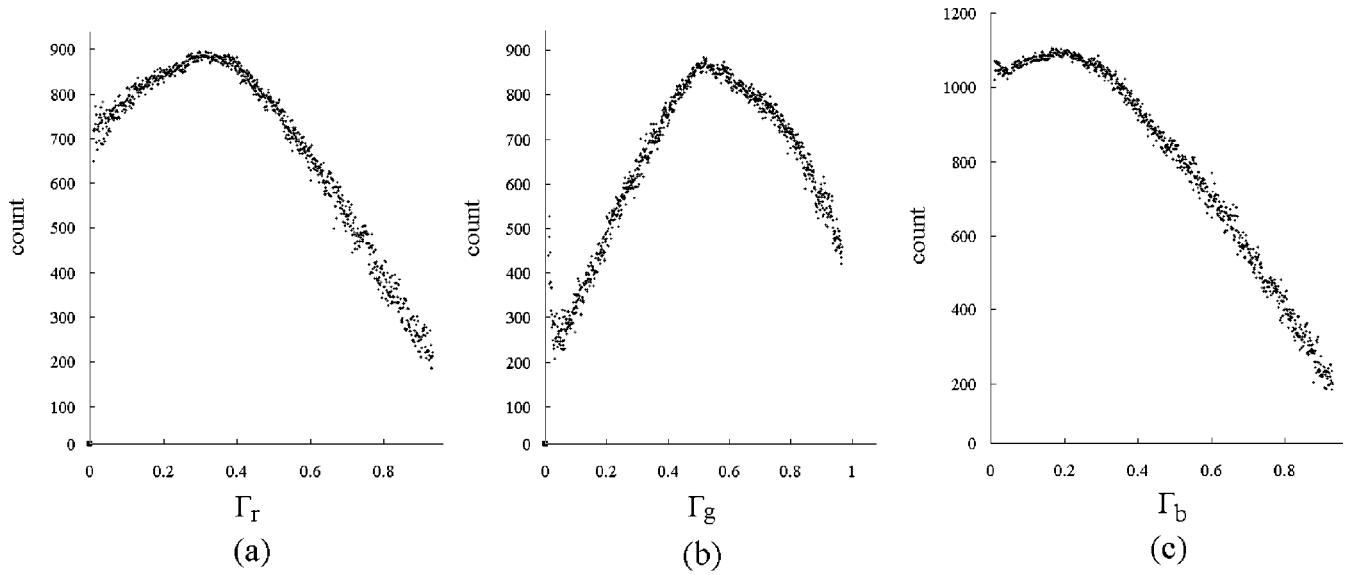

Fig. 14. (a) Intersection-counting distribution for the red channel of illumination chromaticity for the image in Fig. 13, (b) intersection-counting distribution for the green channel, (c) intersection-counting distribution for the blue channel.

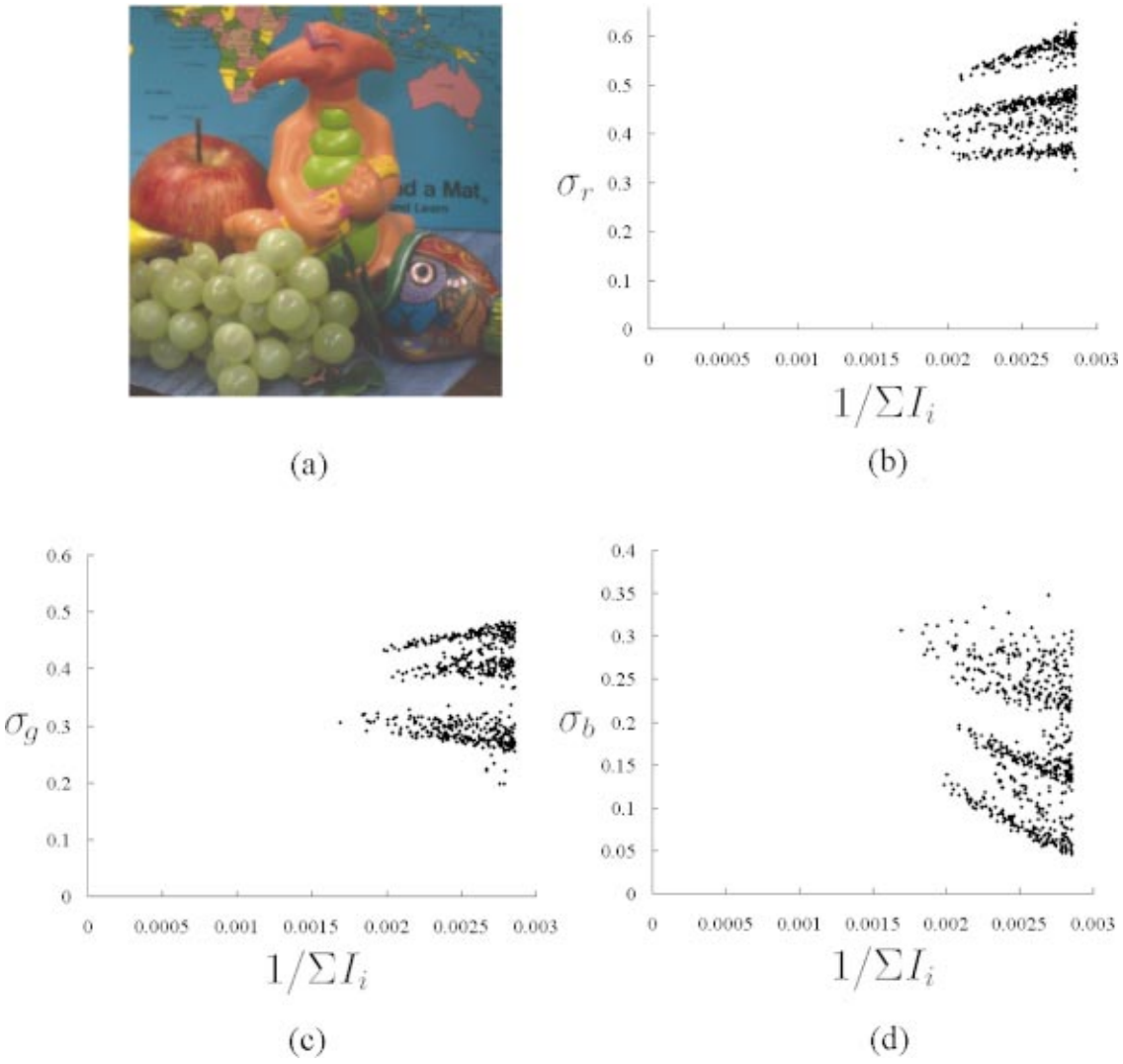

Fig. 15. (a) Real input image of a scene with multiple objects; (b) result of projecting the specular pixels into inverse-intensity chromaticity space, with c representing the red channel; (c) result of projecting the specular pixels, with c representing the green channel; (d) result of projecting the specular pixels, with c representing the blue channel.

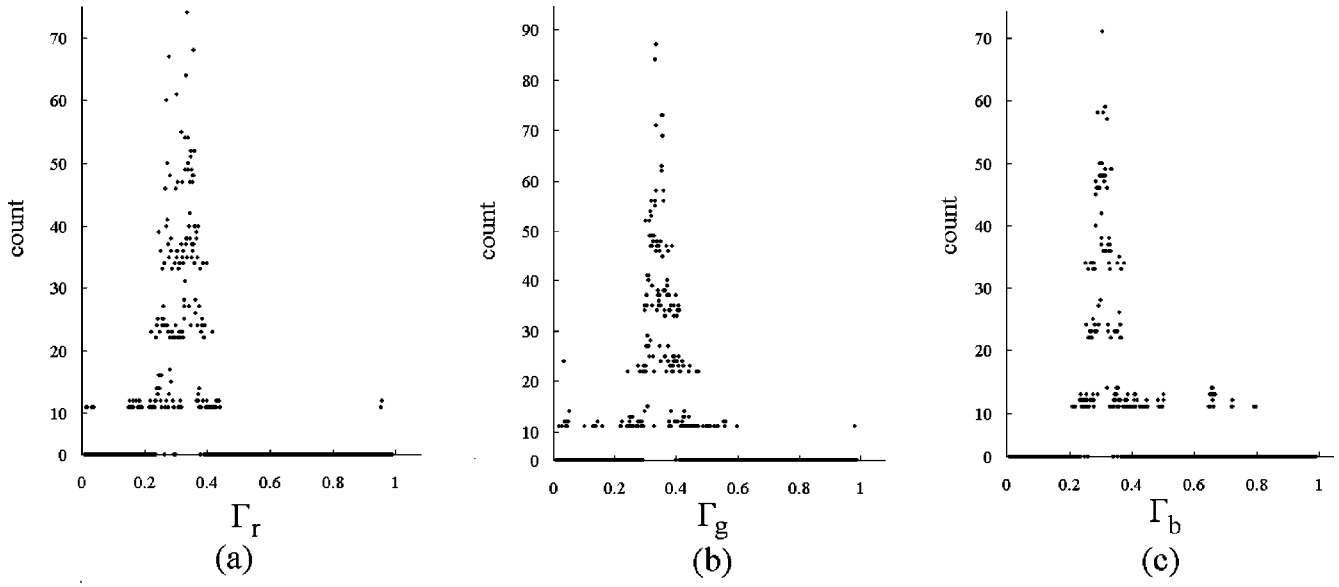

Fig. 16. (a) Intersection-counting distribution for the red channel of illumination chromaticity for the image in Fig. 13, (b) intersection-counting distribution for the green channel, (c) intersection-counting distribution for the blue channel.

Figure 9(b) shows the specular points of the red channel of chromaticity in inverse-intensity chromaticity space. Even though there is some noise, generally, all points form several straight lines heading for a certain point in the chromaticity axis. The same phenomenon can also be observed in Figs. 9(c) and 9(d). Figure 10 shows the intersection-counting distribution in the illumination-chromaticity count space. The peaks of the distribution denote the illumination chromaticity. The result of the estimation was $\Gamma_r = 0.378$, $\Gamma_g = 0.324$, $\Gamma_b = 0.287$.

Result on a multicolored surface. Figure 11(a) shows a plastic toy with a multicolored surface. The illumination is a Solux Halogen covered with a green filter. The image chromaticity of the white reference under this illuminant taken by our camera was $\Gamma_r = 0.298$, $\Gamma_g = 0.458$, $\Gamma_b = 0.244$.

Figures 11(b)–11(d) show the specular points of multiple surface colors in inverse-intensity chromaticity space. From Fig. 12, we can observe that, even for several surface colors, the peak of intersection counts was still at a single value of Γ_c. The result of the estimation was $\Gamma_r = 0.319$, $\Gamma_g = 0.439$, $\Gamma_b = 0.212$.

Result on a highly textured surface. Figure 13(a) shows a magazine cover with a complex multicolored surface, which was lit by a fluorescent light covered with a green filter. The image chromaticity of the white reference under this illuminant taken by our camera has a chromaticity value of $\Gamma_r = 0.283$, $\Gamma_g = 0.481$, $\Gamma_b = 0.236$. The result of the estimation was $\Gamma_r = 0.315$, $\Gamma_g = 0.515$, $\Gamma_b = 0.207$. (See Fig. 14.)

Result on multiple objects. Figure 15(a) shows a scene with multiple objects, which was lit by a fluorescent light taken in an uncontrolled environment. The image chromaticity of the white reference under this illuminant taken by our camera has a chromaticity value of $\Gamma_r = 0.337$, $\Gamma_g = 0.341$, $\Gamma_b = 0.312$. The result of the estimation was $\Gamma_r = 0.321$, $\Gamma_g = 0.346$, $\Gamma_b = 0.309$. (See Fig. 16.)

Evaluation. To evaluate the robustness of our method, we also conducted experiments on six different objects: two objects with a single surface color, one object with multiple surface colors, and three objects with highly textured surfaces. The illuminants were grouped into five different colors: Solux halogen lamp with temperature 4700 K, incandescent lamp with temperature of approximately 2800 K, and Solux halogen lamps covered with green, blue, and purple filters. The illuminants were arranged at various positions. The total number of images in our experiment was 43. From these images, we calculated the errors of the estimation by comparing them with the image chromaticity of the white reference, which are shown in Table 1. The errors are considerably small, as the standard deviations of the reference image chromaticity are approximately 0.01–0.03. In addition, we also used the database of Lehmann and Palm[23] to evaluate the accuracy and the robustness of our method. The database contains various colors of multiple objects. Table 2 shows the results of our estimation. Besides advancing Lehmann and Palm's method[23] in handling uniformly colored surfaces and highly textured surfaces, the results also show that our method is more stable for general conditions of illumination colors and input images (unclipped/clipped images).

Table 1. Performance of the Estimation Method with Regard to the Image Chromaticity of the White Reference

Error Characteristics	Red	Green	Blue
Average	0.0172	0.0141	0.0201
Standard deviation	0.01	0.01	0.01

7. CONCLUSION

We have introduced a novel method for illumination-chromaticity estimation. The proposed method can handle both uniform and nonuniform surface color objects. Given crude highlight regions, the method can estimate illumination color without requiring color segmentation. It is also applicable for multiple objects with various colored surfaces, as long as there are no interreflections. In this paper, we also introduced inverse-intensity chromaticity space to analyze the relationship between illumination chromaticity and image chromaticity. There are a few advantages of the method. First is the capability to cope with either a single surface color or multiple surface colors. Second, color segmentation inside highlight regions and intrinsic camera characteristics are not required. Third, the method does not use strong constraints on illumination, which several existing color constancy methods, such as a blackbody radiator, use. The experimental results have shown that the method is accurate and robust even for highly textured surfaces.

ACKNOWLEDGMENTS

This research was, in part, supported by Japan Science and Technology (JST) under the CREST Ikeuchi Project.

Table 2. Estimation Results Using the Database of Lehmann and Palm

Illumination	Average of Γ_r	Std. Dev. of Γ_r	Average of Γ_g	Std. Dev. of Γ_g
Unclipped, white	0.320	0.02	0.329	0.02
Clipped, white	0.318	0.02	0.332	0.02
Unclipped, yellow	0.479	0.02	0.411	0.02
Clipped, yellow	0.469	0.02	0.399	0.02

REFERENCES

1. G. F. Finlayson and G. Schaefer, "Solving for colour constancy using a constrained dichromatic reflection model," Int. J. Comput. Vision **42**, 127–144 (2001).
2. D. H. Brainard and W. T. Freeman, "Bayesian color constancy," J. Opt. Soc. Am. A **14**, 1393–1411 (1997).
3. G. D. Finlayson, "Color in perspective," IEEE Trans. Pattern Anal. Mach. Intell. **18**, 1034–1036 (1996).
4. G. D. Finlayson, S. D. Hordley, and P. M. Hubel, "Color by correlation: a simple, unifying framework for color constancy," IEEE Trans. Pattern Anal. Mach. Intell. **23**, 1209–1221 (2001).
5. C. Rosenberg, M. Hebert, and S. Thrun, "Color constancy using KL-divergence," in *Proceedings of the IEEE International Conference on Computer Vision* (Institute of Electrical and Electronics Engineers, New York, 2001), pp. 239–247.
6. G. Sapiro, "Color and Illumination Voting," IEEE Trans. Pattern Anal. Mach. Intell. **21**, 1210–1215 (1999).
7. S. Tominaga, S. Ebisui, and B. A. Wandell, "Scene illuminant classification: brighter is better," J. Opt. Soc. Am. A **18**, 55–64 (2001).
8. S. Tominaga and B. A. Wandell, "Natural scene-illuminant estimation using the sensor correlation," Proc. IEEE **90**, 42–56 (2002).
9. M. D'Zmura and P. Lennie, "Mechanism of color constancy," J. Opt. Soc. Am. A **3**, 1162–1672 (1986).
10. G. D. Finlayson and B. V. Funt, "Color constancy using shadows," Perception **23**, 89–90 (1994).
11. B. V. Funt, M. Drew, and J. Ho, "Color constancy from mutual reflection," Int. J. Comput. Vis. **6**, 5–24 (1991).
12. H. C. Lee, "Method for computing the scene-illuminant from specular highlights," J. Opt. Soc. Am. A **3**, 1694–1699 (1986).
13. H. C. Lee, "Illuminant color from shading," in *Physics-Based Vision Principle and Practice: Color* (Jones and Bartlett, Boston, Mass., 1992), pp. 340–347.
14. G. F. Finlayson and S. D. Hordley, "Color constancy at a pixel," J. Opt. Soc. Am. A **18**, 253–264 (2001).
15. J. M. Geusebroek, R. Boomgaard, S. Smeulders, and T. Gevers, "A physical basis for color constancy," in *Proceedings of the First European Conference on Colour in Graphics, Image and Vision* (Society for Imaging Science and Technology, Springfield, Va., 2002), pp. 3–6.
16. J. M. Geusebroek, R. Boomgaard, S. Smeulders, and H. Geert, "Color invariance," IEEE Trans. Pattern Anal. Mach. Intell. **23**, 1338–1350 (2001).
17. H. J. Andersen and E. Granum, "Classifying illumination conditions from two light sources by colour histogram assessment," J. Opt. Soc. Am. A **17**, 667–676 (2000).
18. S. Shafer, "Using color to separate reflection components," Color Res. Appl. **10**, 210–218 (1985).
19. G. J. Klinker, S. A. Shafer, and T. Kanade, "The measurement of highlights in color images," Int. J. Comput. Vis. **2**, 7–32 (1990).
20. G. J. Klinker, "A physical approach to color image understanding," PhD. thesis (Carnegie Mellon University, Pittsburgh, Pa., 1988).
21. S. Tominaga, "A multi-channel vision system for estimating surface and illumination functions," J. Opt. Soc. Am. A **13**, 2163–2173 (1996).
22. S. Tominaga and B. A. Wandell, "Standard surface-reflectance model and illumination estimation," J. Opt. Soc. Am. A **6**, 576–584 (1989).
23. T. M. Lehmann and C. Palm, "Color line search for illuminant estimation in real-world scene," J. Opt. Soc. Am. A **18**, 2679–2691 (2001).
24. G. D. Finlayson and G. Schaefer, "Convex and non-convex illumination constraints for dichromatic color constancy," in *Proceedings of the IEEE Conference on Computer Vision and Pattern Recognition* (IEEE, New York, 2001), pp. 598–605.
25. G. Healey, "Using color for geometry-insensitive segmentation," J. Opt. Soc. Am. A **6**, 920–937 (1989).
26. H. C. Lee, E. J. Breneman, and C. P. Schulte, "Modeling light reflection for computer color vision," IEEE Trans. Pattern Anal. Mach. Intell. **12**, 402–409 (1990).
27. J. H. Lambert, *Photometria sive de mensura de gratibus luminis, colorum et umbrae* (Eberhard Klett, Augsberg, Germany, 1760).
28. K. E. Torrance and E. M. Sparrow, "Theory for off-specular reflection from roughened surfaces," J. Opt. Soc. Am. **57**, 1105–1114 (1967).